*Earth Planets Space*, **59**, 437–451, 2007

# Spectroscopic measurements of Si-O recombination process in laser-induced quartz vapor plumes

Masanori Fuyuki[1*], Seiji Sugita[1], Toshihiko Kadono[2], Sunao Hasegawa[3], and Takafumi Matsui[1]

[1]*Department of Complexity Science and Engineering, University of Tokyo, 5-1-5 Kashiwanoha, Kashiwa, Chiba 277-8561, Japan*
[2]*Institute for Frontier Research on Earth Evolution, Japan Marine Science and Technology Center, 2-15 Natsushima-cho, Yokosuka-city, Kanagawa 237-0061, Japan*
[3]*Research Division for Planetary Science, The Institute of Space and Astronautical Science, 3-1-1 Yoshinodai, Sagamihara, Kanagawa 229-8510, Japan*

(Received September 20, 2003; Revised June 9, 2006; Accepted January 16, 2007; Online published June 8, 2007)

The thermal dissociation of $SiO_2$ in impact-induced vapor is very important because it controls the redox state of the vapor. However, the thermal dissociation of $SiO_2$ and its recombination are not well understood. The present study investigates experimentally the kinetics of the Si-O recombination process at high temperatures. Laser-induced quartz vapor is observed by means of time-resolved spectroscopy, and the atomic lines of Si and molecular bands of SiO are measured in order to estimate the temperature and the column densities of Si and SiO. The results of these experiments show that Si and O recombine as the vapor cools from 5000 to 3000 K. A comparison of the observed chemical composition and equilibrium calculations suggests that the recombination reaction between Si and O proceeds rather efficiently under a condition that differs significantly from the thermochemical equilibrium. This result is explained well if the rate constant of the Si-O recombination process does not depend strongly on the temperature; the activation energy is very small. These results suggest that the Si-O recombination process may not be approximated by a frequently-used 'freeze-out' model.

**Key words:** Si-O recombination process, laser-induced quartz vapor plume, time-resolved spectroscopy, Si atomic lines, SiO molecular bands, chemical equilibrium calculation, activation energy.

## 1. Introduction

The heavy bombardment of planetesimals is considered to have occurred during the early stage of the Earth's history (e.g., BVSP, 1981). The degassing of these planetesimals during impacts resulted in the release of volatiles. An important aspect of vaporization of silicates, as opposed to degassing of volatile components, is the thermal dissociation of $SiO_2$. Mukhin *et al*. (1989) suggested that molecular oxygen released by the thermal dissociation of $SiO_2$ in an impact-induced vapor plume may play an important role in controlling the redox state of carbon and metals and, consequently affect the origin and evolution of planetary atmospheres and life.

In addition to the asteroids and comets, small particles—the so-called interplanetary dust particles (IDP's)—constantly impact the surface of airless bodies, such as asteroids and the moon (e.g., Divine, 1993; Sasaki *et al*., 2001). Since the main component of IDP's is silicate, the dissociation of $SiO_2$ in such small-size vapor plumes also plays an important role in the formation of the regolith on the lunar surface.

The recombination process of Si and O atoms to SiO and $O_2$ molecules is the first step in the formation process of $SiO_2$: the second step consists of $SiO + O_2 \rightarrow SiO_2 + O$ or $SiO + O \rightarrow SiO_2$. These reactions take place at very high temperatures. A number of calculations have been conducted to estimate the rate constants of such high-temperature reactions among different molecules. The oxidation process of Al is sometimes used to estimate that of Si. Park (1976) provided the rate constants of gas-phase reactions (including Al, Cl, O, and H) expected to occur among the constituents of the exhaust gas of a solid-fuel rocket engine in the hot region behind the Mach disk. In these rate constants, the activation energy of an exothermic reactions was assumed to be 0 kJ/mol. Park and Arnold (1978) subsequently applied this assumption to these reactions including Si.

The properties of C atoms, such as collisional cross section with other atoms and molecules, are also often used to predict the properties of Si. Fegley *et al*. (1986) provided the rate constants of the reactions relevant to destruction process of CN and HNO by a large impact in the shock-heated atmosphere of the ancient Earth. In their list, the activation energy of the exothermic reactions are not necessarily $\sim$0 kJ/mol, but the value depends on the reactants. In other words, some rate constants depend on temperature exponentially and some others do not. Given this background, it is therefore impossible to predict whether the rate constant of the Si-O recombination process and that of SiO-O have $\sim$0 kJ/mol activation energy based solely on a comparison with other elements.

*Now at Genesis Research Institute, Inc., Futamata 717-86, Chiba 272-0001, Japan.

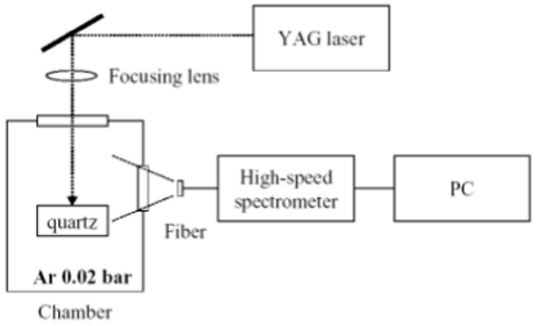


Fig. 1. A schematic diagram of our experimental system.

Using *ab initio* calculation, Andreazza *et al*. (1995) estimated the rate constant of the recombination of Si and O and found that it does not depend on the temperature exponentially and that the activation energy of the process is ∼0 kJ/mol. In their calculation, the Si-O recombination is assumed to be a radiative association reaction.

The objective of the experiments reported here was to investigate empirically whether the rate constant of the Si-O recombination process is strongly temperature dependent; i.e., whether the activation energy of the process is practically 0 kJ/mol or significantly higher than 0 kJ/mol.

Small activation energy as this has a very important implication to planetary science. Silicates in impact-induced vapor plumes are often assumed to condense and essentially to go outside the chemical reaction system at very high temperatures and to have no influence on the subsequent chemical reactions among volatile elements, such as C, N, and H, at lower temperatures. This is based on a so-called 'freeze-out' model. In this model, when the temperature is higher than the quenching temperature, the chemical composition is given by the equilibrium composition at that temperature. When the temperature goes below the quenching temperature, the chemical reaction stops suddenly; consequently, the chemical composition becomes fixed at the quenching temperature, and freeze-out occurs. However, such a freeze-out model works only if the activation energy of the reaction is high. If the activation energy is small, such a sudden cessation of the chemical reaction does not occur and a freeze-out model is not applicable.

In the experiments described here, we used a pulsed laser to heat quartz (i.e., $SiO_2$) to produce a vapor of Si and O atoms. Then the resulting vapor plumes were then observed using a high-speed spectrometer. Based on our analysis of the spectroscopic data, we estimated a change in the chemical composition during expansion and cooling of the plume. We also calculated the equilibrium chemical composition of the high-temperature vapor and compared it with the observed chemical composition. Taking the cooling rate of the vapor and the number ratio of reactants and products into consideration, we discuss how the rate constant of Si-O recombination reaction is temperature-dependent.

## 2. Experiments

### 2.1 Experimental condition

Our experimental system is schematically shown in Fig. 1. A quartz sample was placed in a vacuum chamber filled with argon (0.02 bar). Argon does not react with the chemical compounds in the resulting vapor but it does slow the expansion speed of vapor, thereby allowing more time for spectroscopic observation. The sample was exposed to a Nd:YAG laser pulse (wavelength: 1.06 $\mu$m, energy per pulse: 380 mJ, and pulse width: 15 ns). The diameter of the irradiation spot was 2 mmand, therefore, the power density of the beam was about $10^9$ W/cm$^2$. Laser-induced vapor plumes were observed using a high-speed spectrometer (PI-MAX 1024, Prinston Instruments.). The wavelength of the spectrometer was calibrated using a Hg lamp, and observation were made between 160 nm and 440 nm. The full width of the half maximum (FWHM) of the instrumental function of our system is 0.90 nm. For the intensity calibration, we used a Xenon lamp (Hamamatsu Photonics Inc., model L7810). Exposure of the spectrometer was triggered by a photodiode that captures the laser light scattered on the target. The rise time of the photodiode is 5 ns.

### 2.2 Experimental results

About 10–20 mg of the quartz sample was lost after the sample had been exposed 1000 times to the laser pulse. Figure 2 shows the observed spectra as a function of time after the laser irradiation. In order to improve the signal-to-noise (S/N) ratio, more than 100 pieces of data were added together under the same irradiation conditions. Immediately after a laser irradiation, blackbody radiation and ionized argon lines were observed (Fig. 2(a)). The Argon II lines indicate the presence of ionized plasma and the possible non-thermal acceleration of the plume by the electron cloud during the earliest stage of a laser-induced plume. Several microseconds after the irradiation, the spectra of Si and SiO produced by the dissociation of $SiO_2$ appeared (Fig. 2(b)). Emission bands between 250 and 300 nm are those of SiO Main System. All of the spectra shown in Fig. 2 (b)–(d) are normalized with the intensity of the Si line spectrum at 288 nm. In the observation period between 20 and 100 $\mu$s, the blackbody radiation was not as strong as the Si line emissions or SiO band emissions, indicating that the vapor expanded and that condensates are not the main components of the vapor plume but that the gas phase is dominant during this period of time. We found that the normalized intensity of the SiO spectra increased with time, suggesting that Si and O were recombining rapidly and that the oxygen fugacity in the vapor plume decreased rapidly as the vapor cooled down. Atomic oxygens emit their line spectrum strongly at 777 nm (Wiese and Martin, 1980), but this wavelength is far from the region where SiO molecules emit their band spectra. The ICCD detector is also very insensitive to such a long wavelength. In order to observe emission spectrum with high enough spectral resolution to analyze observed spectra, we focused on observing the spectra of Si and SiO in the UV wavelength range. After the observation, we examined the inside of the chamber and found condensates around the sample.

## 3. Analysis

In this section, we discuss the analysis of the observed spectra and show how the number ratio of Si to SiO changes as the temperature in the vapor plume decreases. To do this, we use the following equation to derive the number ratio

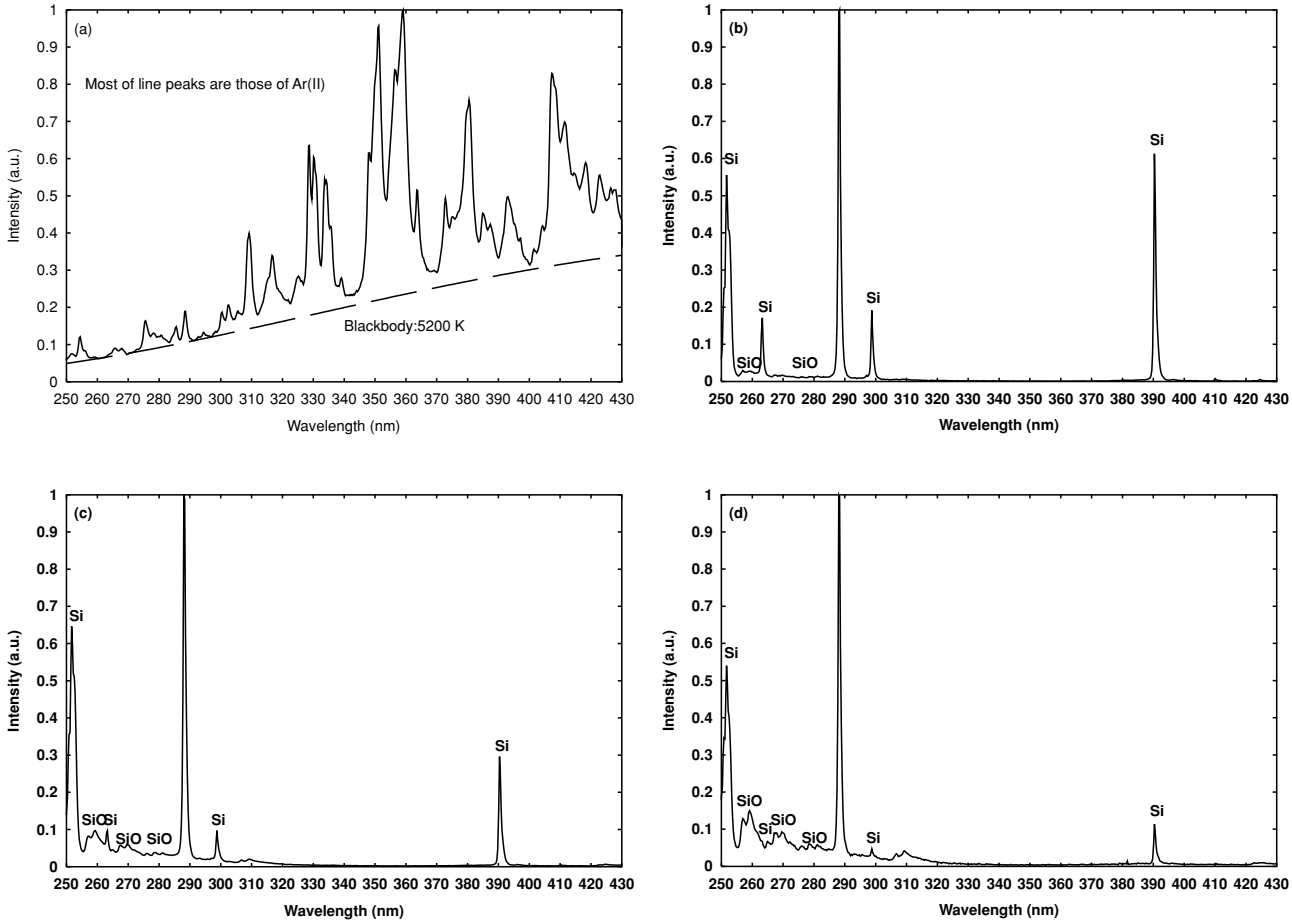


Fig. 2. Observed emission spectra as a function of time after the laser irradiation. Exposure time for each spectrum is: (a) 10–13 ns, (b) 20–21 $\mu$s, (c) 40–60 $\mu$s, (d) 80–100 $\mu$s. The number of data added together for each condition is: (a) 100, (b) 500, (c) 500, (d) 500. The intensity scale for the spectra in Fig. 2(b)–(d) is normalized by Si line spectrum at 288.1 nm. The band emissions at 307 nm and 310 nm in Fig. 2(d) are those of NO due to contamination of Air.

of Si to SiO from the ratio of spectral intensity of Si line emission to SiO band emission.

$$\frac{N_{\mathrm{Si}}}{N_{\mathrm{SiO}}} = \frac{I_{\mathrm{Si}}}{I_{\mathrm{SiO}}} \frac{E_{\mathrm{SiO}}}{E_{\mathrm{Si}}} \exp\left(\tau_{\mathrm{SiO}} - \tau_{\mathrm{Si}}\right) \tag{1}$$

where $N_{\mathrm{Si}}$ and $N_{\mathrm{SiO}}$ are the number densities of each species, $I_{\mathrm{Si}}$ and $I_{\mathrm{SiO}}$ are the intensities of observed spectra, $E_{\mathrm{Si}}$ is an intensity of the theoretical emission spectrum from a Si atom without self-absorption, and $E_{\mathrm{SiO}}$ is an intensity of the theoretical emission spectrum from a SiO particle without self-absorption. The symbols $\tau_{\mathrm{Si}}$ and $\tau_{\mathrm{SiO}}$ denote the optical thickness of Si and SiO, respectively.

The first step is to measure the temperature of the vapor in the earliest stage of vapor expansion based on the blackbody radiation observed. The second step is to estimate the temperature of Si at different observation times based on the intensities of Si lines, followed by and estimation of the temperature based on the SiO spectral pattern. Unlike Si spectra, each rotational line in the SiO band cannot be spectrally separated. The temperature and column density of SiO are then estimated simultaneously. The optical thickness $\tau_{\mathrm{SiO}}$ of the SiO Main system is calculated based on the estimated temperature and column density, and the emission intensities $E_{\mathrm{Si}}$ and $E_{\mathrm{SiO}}$ are then calculated as functions of temperature. Using these values, we are able to determine the number ratio of $N_{\mathrm{Si}}/N_{\mathrm{SiO}}$ at different observation periods.

### 3.1 The initial vapor temperature

During the first few microseconds after laser irradiation, the blackbody radiation from the dense vapor was so strong that its shape could be used to estimate the temperature (Fig. 2(a)). Comparing theoretical spectra of blackbody radiation with the observed spectra, we found that the temperature of the vapor in an early stage is about 5200 K (Fig. 3).

### 3.2 The temperature of Si

Emission lines of Si appeared at 5 $\mu$s after laser irradiation (Fig. 2(b)). Using optically thin spectral lines, we are able to measure the excitation temperature of atoms (Griem, 1964; Sugita *et al.*, 1998). However, when there is a large population of atoms in the lower energy level of the electronic transition that associate with a line emission, the line becomes optically thick and self-absorption occurs (Griem, 1964; Cannon, 1985; Sugita *et al.*, 1998).

Figure 4 shows the upper and lower energy levels of electronic transition for the spectral lines of Si shown in Fig. 2. Because the vapor plume observed is expected to cool, the temperature should be below the initial temperature of 5200 K obtained from blackbody spectrum (the gray zone in Fig. 4). This energy level distribution helps us predict which emission line has strong self-absorption

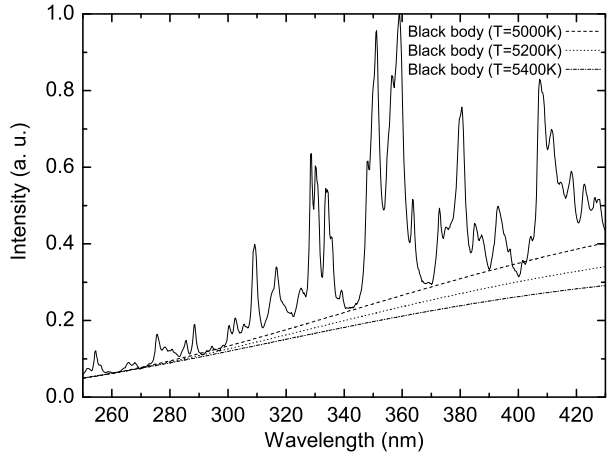


Fig. 3. The blackbody radiation obtained in the early stage of observation (10–13 ns) and Plank functions at various temperatures. Note that the functions are scaled to fit the intensity of the observed spectrum at 260 nm.

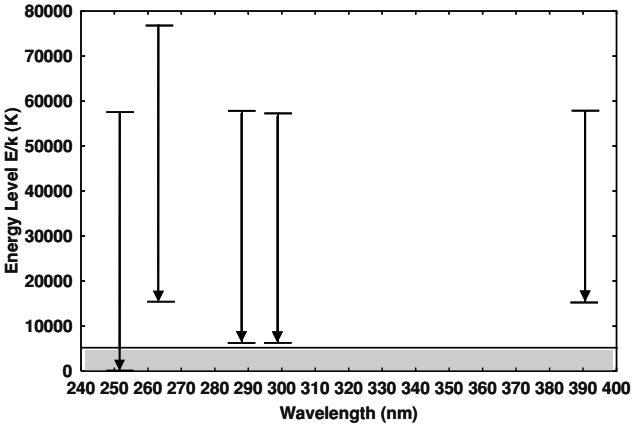


Fig. 4. The upper and lower energy levels of electronic transitions for line emissions of Si. The gray zone shows the region of the temperature the vapor plume is expected to experience during expansion.

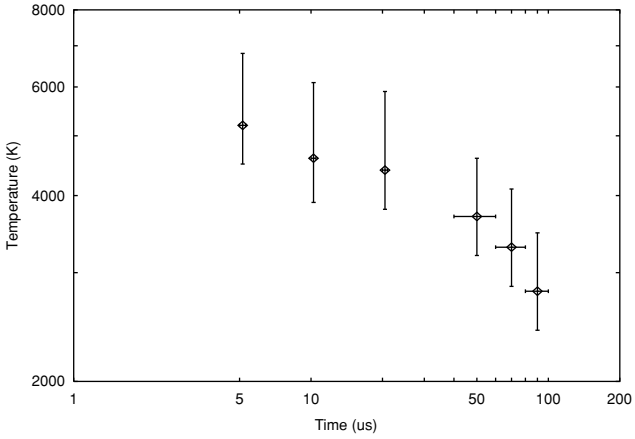


Fig. 5. The excitation temperature of Si measured as a function of time. The data show that the vapor plume cools monotonically.

and which line does not.

Using optically thin Si spectral lines, we can measure the excitation temperature of Si. Since the lower energy levels of the spectral lines at 263 nm and 391 nm are much higher than the gray zone in Fig. 4, the populations of the these energy levels are much smaller than unity throughout the observation period. We assume that the lines are well thermalized. In a thermodynamic equilibrium, the populations of these states are given by a Boltzmann distribution: $g\exp(-E/kT)/Z$, where $Z$, $g$, $E$, $k$, and $T$ are partition function, statistical weight, energy level of a state, Boltzmann constant, and temperature, respectively. The population of the lower energy levels of the line at 263 nm and that of the line at 391 nm are the same; $\exp(-15394.24/T)/Z$ (Wiese and Martin, 1980). The vapor we observed was expected to cool and fall below the initial temperature of 5200 K during our observation. In this range of temperature, the partition function $Z$ is approximately unity. In the vapor we observed, the ratio of the population of the energy level to the total number of atom Si in the vapor plume was then expected to be less than 0.05. As the temperature decreases, this population ratio will decrease furthermore. Thus spectra lines at 263 nm and 391 nm are most likely to be optically thin. Assuming that the lines are well thermalized, we can use them to estimate the excitation temperature. Figure 5 shows the temperature measured as a function of time. The data show that the vapor plume cooled monotonically throughout the observation time.

### 3.3 The temperature and column density of SiO

Although the SiO band spectrum consists of many individual rotational lines, it appeared as a continuous band spectrum with our limited spectral resolution. Thus it was impossible to estimate the temperature and the column density by measuring individual rotational lines of SiO. In order to estimate those quantities, we calculated the synthetic spectrograms of the SiO emission band at different temperatures and densities and searched for the optimum temperature and column density that minimize the difference between the synthetics and the observed spectrum in the laser experiments.

There are three steps in such calculations (e.g., Sugita and Schultz, 2003). The first step is to calculate a "source" spectrum, i.e., emission intensity per a unit mass of SiO molecules. This step considers all of the rotational lines and the effects of line broadening but neglects self-absorption. The second step is to calculate the effect of self-absorption, and the third step is to assess the effect of the finite spectral resolution of spectrometers. The details of the procedures are given in Appendix A.

When a synthetic spectrogram is calculated, the result of the synthetic calculation can be compared with experimental results. As such the optimum temperature and column density of SiO that minimize the difference between an experimental spectrum and a theoretical spectrum can then be determined.

The spectral pattern of theoretical synthetics is controlled by both the temperature and the column density of SiO molecules and the Lorentz/Doppler broadening ratio $\alpha$. The ratio $\alpha$ is different for each rotational line of a source spectrum (see Appendix B). Here we use the ratio $\alpha$ for the rotational line at 270 nm as the reference ratio $\alpha$. For different values of these controlling parameters, we calculated

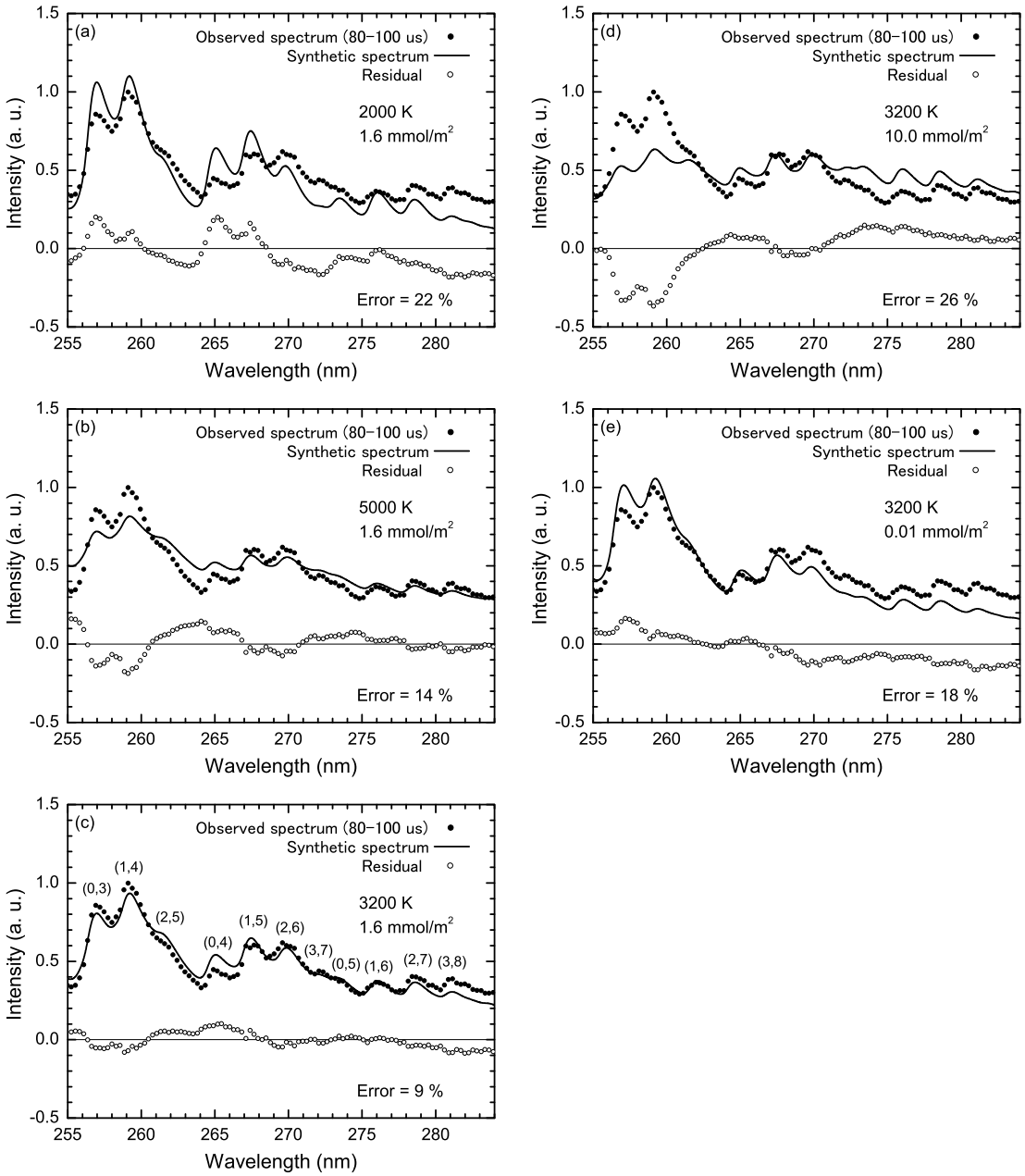


Fig. 6. Comparison between an observed spectrum and several theoretical synthetics of the SiO Main System with various model parameters. The bands of strong intensities are separated into three parts by $\Delta v$. The observed spectrum was obtained in the observation period between 80 $\mu$s and 100 $\mu$s. The calculation is only for a single value of the line-broadening ratio $\alpha$ of 0.1.

a synthetic spectrum and compared this with an observed spectrum. The degree of similarity was assessed with the square mean $E_r$ of the difference defined as

$$E_r = \frac{\int \left[I_{syn}(\lambda) - I_{obs}(\lambda)\right]^2 d\lambda}{\int \left[I_{obs}(\lambda)\right]^2 d\lambda} \qquad (2)$$

where $I_{syn}$ and $I_{obs}$ are a synthetic and an observed spectra, respectively (e.g., Sugita and Schultz, 2003). The combination of the parameters that minimizes the error $E_r$ is considered to be the optimum condition to describe an observed emission spectrum.

A comparison between an observed spectrum of the SiO Main System and theoretical synthetics with different controlling parameters is shown in Fig. 6. The bands of strong intensities are separated into three parts with different $\Delta v$, where $\Delta v$ is the difference in vibrational quantum number between the upper and lower states associated with the emission. When too low a temperature is used for a synthetic calculation, the intensities of the band heads at shorter wavelengths of each part become too high, whereas those at longer wavelengths become too low (Fig. 6(a)). When too high a temperature is used, the intensities of the band heads at shorter wavelengths of each part become too low, whereas those at longer wavelengths become too high (Fig. 6(b)). Only when an optimum temperature is chosen can the pattern of intensity be reproduced with a small error (Fig. 6(c)). Note that the intensity of a synthetic spectrum is optimally scaled in such a way that the mean square difference $E_r$ with the observation may be minimized.

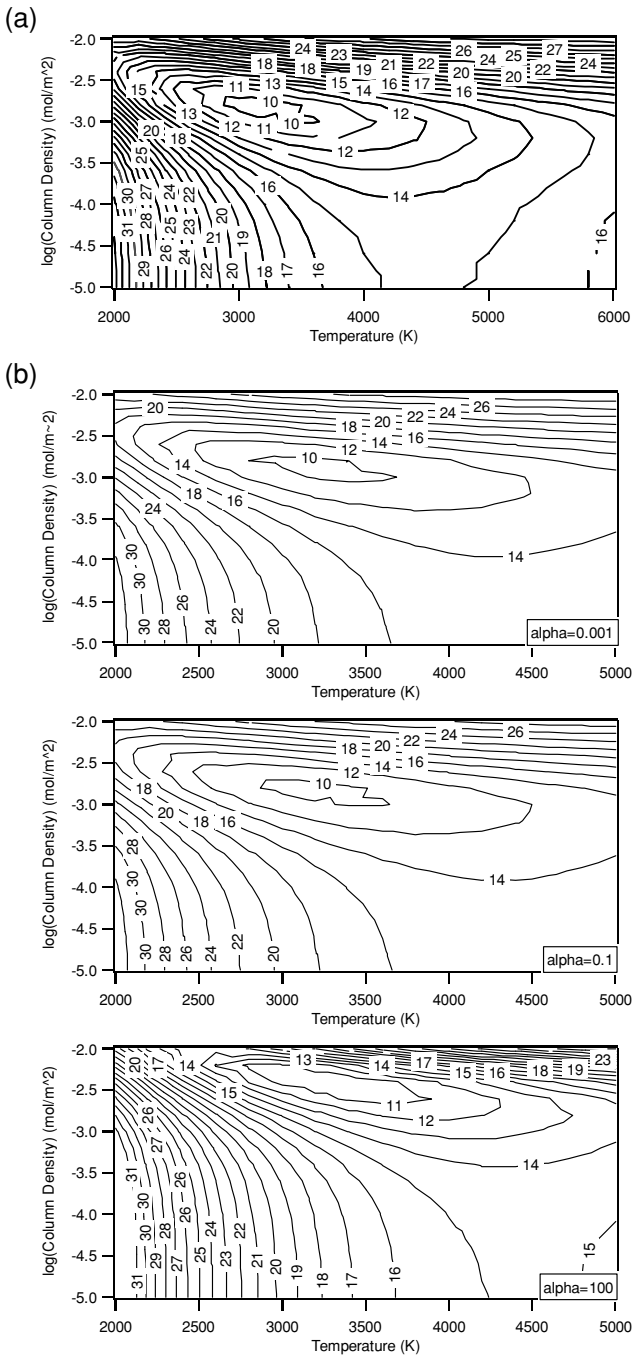


Fig. 7. (a) Contour map of the square mean error (%) of synthetic spectra as a function of both temperature and column density of SiO molecules. The observed spectrum shown in Fig. 6 is used here for the analysis. The minimum error is given by the temperature of 3200 K and column density of 1.6 mmol/m$^2$. This error analysis assumes the ratio of line-broadening factor $\alpha$ of 0.1. The optimum temperature depends only a little on $\alpha$, and the optimum column density depends somewhat on $\alpha$. (b) Contour maps of the square mean error (%) of synthetic spectra as a function of both temperature and column density of SiO molecules. The observed spectrum shown in Fig. 6 is used here for the analysis. The line broadening ratio $\alpha$ for each estimation is indicated in the figures. These figures show how the optimum set of temperature and column density depends on $\alpha$. The optimum temperature depends only a little on $\alpha$, and the optimum column density depends somewhat on $\alpha$.

When too large or too low a value of column density of SiO molecules is used, a synthetic spectrum with the optimum temperature fails to resemble the observed spectrum.

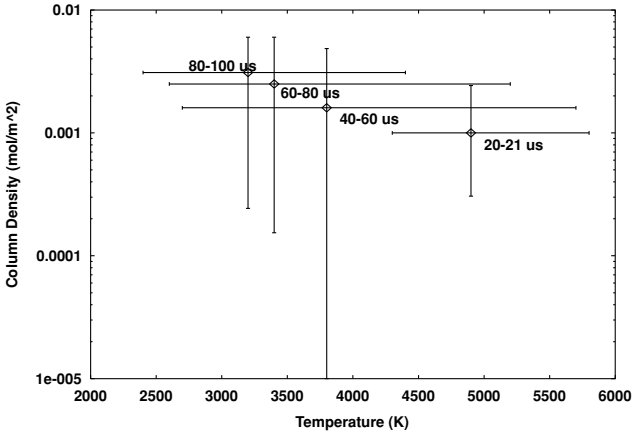


Fig. 8. The temperature and column density derived from SiO molecular radiation. The data points denoted by diamonds in the figure are observed 20–21 $\mu$s, 40–60 $\mu$s, 60–80 $\mu$s, and 80–100 $\mu$s after the laser irradiation, respectively from the right to the left. The temperature and column density with the square mean $Er$ of the difference smaller than 12% are considered to be the optimum. The vertical error bars are estimated by the uncertainty in the electronic transition probability (30%) and that in the line-broadening ratio $\alpha$. With larger $\alpha$, the optimal column density becomes higher. The data points denoted by diamonds on each cross indicates the values when $\alpha$ is assumed 1.0. Horizontal errors are estimated by only the square mean $Er$.

A gas body emits the blackbody radiation when the source spectrum is fully self-absorbed. Since the optimum temperature in our study was relatively low (i.e., 3200 K), the intensity of blackbody radiation was stronger at a longer wavelength within the range (250–430 nm) covered. When too large a value of column density was used, the spectrum of SiO became close to the blackbody radiation (Fig. 6(d)). When too low a value of column density was used, the opposite occured; i.e., the intensity at the shorter wavelength became stronger and that at the longer wavelength became weaker (Fig. 6(e)). Consequently, both temperature and self-absorption changed the shape of the emission spectrum, and the effects of the two parameters were different. Thus a quantitative analysis can determine simultaneously the optimum values of both temperature and column density.

The square mean $Er$ of the difference for the same observed spectrum is shown in Fig. 7(a) as a function of both the temperature and column density of SiO molecules. Figure 7(a) shows that the optimum temperature and column densities are about 3200 K and 1.6 mmol/m$^2$, respectively. In our analysis, the temperature and column density with the square mean $Er$ of the difference smaller than 12% are treated as optimum. The calculation is only for a single value of the line-broadening factor $\alpha$ of 0.1. The optimum range of temperature depends only very little on $\alpha$, and that of optimum column density depends somewhat on $\alpha$ (Fig. 7(b)). The optimum ranges of temperature and column density as a function of assumed $\alpha$ are calculated for the emission spectrum of each observation period.

A summary of the temperature and column density derived from SiO molecular emission is given in Fig. 8, which shows the temperature and column density of SiO observed at 20–21 $\mu$s, 40–60 $\mu$s, 60–80 $\mu$s, and 80–100 $\mu$s after the

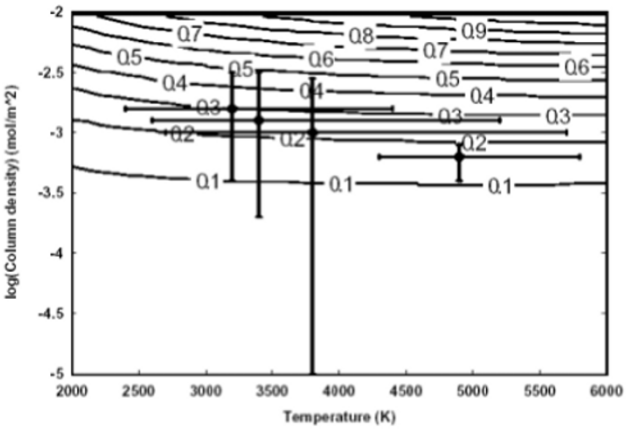


Fig. 9. The optical thickness of synthetic spectra as a function of temperature and column density. The line-broadening ratio $\alpha$ is assumed 0.1. The optimum sets of temperature and column density with the error $Er$ smaller than 12% are also shown in the figure. The observation periods for optimum sets are 20–21 $\mu$s, 40–60 $\mu$s, 60–80 $\mu$s, and 80–100 $\mu$s, respectively from right to left.

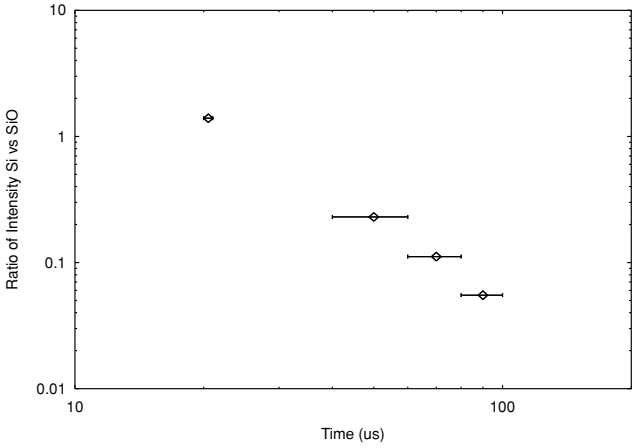


Fig. 10. The ratio of intensity of observed spectra of Si emission line at 391 nm to that of the SiO Main system between 256 nm and 284 nm.

laser irradiation. The optimum sets of temperature and column density with the error $Er$ smaller than 12% are also shown in Fig. 8. The vertical error bars also indicate the uncertainty due to the electronic transition probability (30% (Park *et al.*, 1993)) and the line-broadening ratio $\alpha$. A larger $\alpha$ value leads to a higher column density. It is because line broadening weakens the effect of self-absorption and the column density strengthens the effect. The range of $\alpha$ is determined using the collision rate of Si. The detail is given in Appendix B.

It is to be noted that the column density of SiO was seen to increase as the temperature decreased. This trend cannot be explained by a simple expansion of the vapor without chemical reactions. If the vapor expands without chemical reactions, the column densities of compounds should decrease with temperature. Thus, the observed increase in the column density of SiO indicates that SiO may have resulted from Si-O recombination process in the vapor. This is discussed in detail in Section 4.

### 3.4 The degree of self-absorption of SiO main system

It is necessary to determine the degree of self-absorption of the SiO Main system in order to derive the number ratio of Si to SiO from the ratio of Si line emission intensity to that of SiO band emission (see Eq. (1)). The optical thickness for each observed spectrum was calculated using the optimum temperature and column density determined in Section 3.3. Figure 9 shows the optical thickness $\tau$ of synthetic spectra as a function of temperature and column density. The line-broadening ratio $\alpha$ is assumed to be 0.1. Figure 9 shows that the optical thickness of the SiO Main system is smaller than 0.5. With a larger line-broadening ratio $\alpha$, the optimum column density is lower and the optical thickness does not depend on the ratio. The optical thickness of the SiO Main system fell within the range from 0 to 0.5 during the observation.

### 3.5 The temperatures of Si and SiO

We can now compare the temperatures of Si and SiO (Figs. 5 and 8). These were found to agree well in the observation periods between 40 and 80 $\mu$s. The difference between their central values is less than 200 K. Thus, the Si and SiO we observed are likely to be in the most luminous part of the vapor. However, the Si and SiO temperatures do not agree very well between 20 and 21 $\mu$s and between 80 and 100 $\mu$s. In the spectrum observed during the early stage (i.e., 20–21 $\mu$s), the intensity of the SiO Main system is so weak that its pattern is not observed with a high S/N ratio. Thus the temperature of SiO determined is not very reliable. In the spectrum observed during a late stage (i.e., 80–100 $\mu$s), the line spectrum of Si 263 nm is so weak that the excitation temperature of Si determined has a large uncertainty. Then, we assume that the temperature of Si and that of SiO are the same in the observation periods between 20 and 100 $\mu$s. The excitation temperature of Si used was that of the most luminous part of the vapor between 20 and 21 $\mu$s and the SiO temperature is used was that of vapor between 40 and 100 $\mu$s.

The temperature $T$ of an expanding vapor plume is fitted well by a power-law function of time $t$, $T = A \times t^{-b}$, where $A$ and $b$ are constants (Kadono *et al.*, 2002). The value of $b$ is $0.22 \pm 0.02$ for the vapor plumes observed in this study. A characteristic timescale of the cooling of the vapor $\theta_T$ is given by

$$\theta_T = \left| \frac{(dT/dt)}{T} \right|^{-1}. \quad (3)$$

The cooling rate changes as the vapor cools. The timescale $\theta_T$ depends on the temperature by the power of about $-5.7$.

### 3.6 Si versus SiO in the vapor plume

Figure 10 shows the ratio of the intensity of the Si line at 391 nm to that of the SiO Main system between 256 nm and 284 nm in the observed spectra. This ratio is the ratio $I_{\rm SiO}/I_{\rm Si}$ in Eq. (1). Figure 11 shows the intensities $E_{\rm Si}$ and $E_{\rm SiO}$ of the theoretical emission spectra from a Si atom and a SiO molecule. Using the temperature of the vapor, the ratio $E_{\rm SiO}/E_{\rm Si}$ in Eq. (1) was calculated for each observation period. The optical thickness $\tau$ of Si at 391 nm can be approximated to be 0 (see Section 3.2) and that of the SiO Main system is within the range from 0 to 0.5. Substituting these values into Eq. (1), the number ratio of Si to SiO can be determined. Figure 12 shows the number

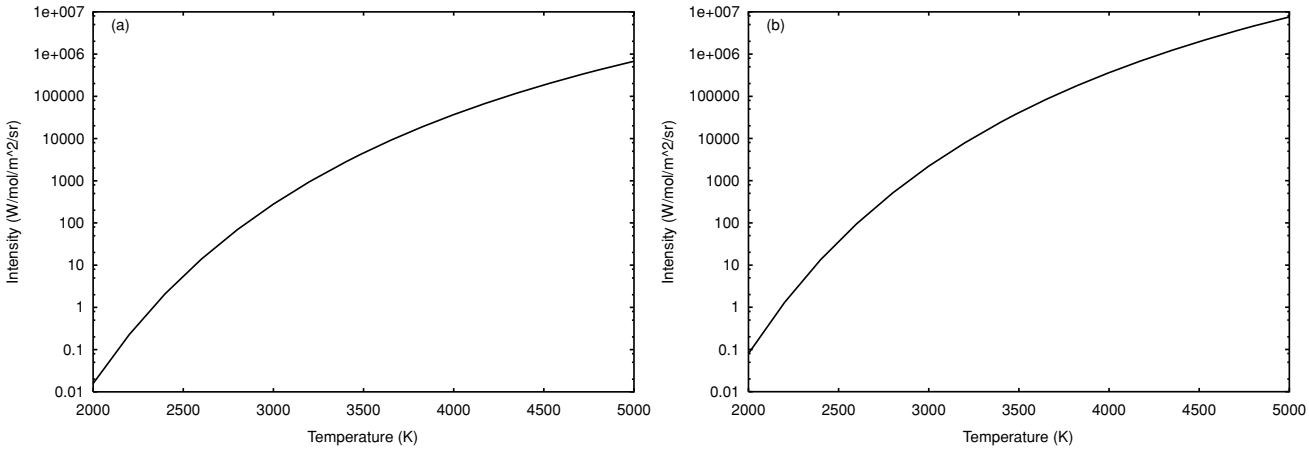


Fig. 11. The intensities of theoretical source spectra from: (a) a Si atom at 391 nm and (b) a SiO molecule between 256 nm and 284 nm.

ratio of Si atoms to SiO molecules as a function of temperature. The monotonic decrease in the Si/SiO ratio strongly suggests that silicon atoms and oxygen atoms recombine to SiO molecules as the temperature decreases.

## 4. Discussion

In this section, we discuss the chemical equilibrium calculation of the Si-O system under possible conditions with the aim of determining whether the observed reaction process is consistent with a chemical-equilibrium model.

### 4.1 The chemical equilibrium of the $SiO_2$ system

We carried out chemical equilibrium calculation using the Gibbs-free-energy minimization method and the JANAF thermo-chemical tables (Chase *et al*., 1985). Since the samples used for the experiments are $SiO_2$ crystals, the calculation system comprises entirely Si and O; the silicon-to-oxygen ratio is 1:2. The following atoms and molecules are included in the calculation: Si(g), SiO(g), $SiO_2$(g), O(g), $O_2$(g), Si(c), $SiO_2$(c). The symbols (g) and (c) indicate gas and condensed phases, respectively. The ideal and Van der Waals equation of state are used for the gas-phase calculation. Note that Van der Waals radius of the $SiO_2$ molecule is much larger than those of the other molecules. We use Van der Waals equation of state only for $SiO_2$ molecule. The critical constants of $SiO_2$ molecule are given by Ahrens and O'keefe (1972).

Figure 13 shows the molar fraction of each compound under a chemical equilibrium as a function of temperature between 2500 and 6000 K at 1 bar. We fix the pressure for this calculation to show how the chemical equilibrium depends on temperature. The value of 1 bar is just a reference pressure between the highest and lowest pressures expected for the vapor. The pressure of the vapor observed is expected to be several thousand bars immediately after the laser irradiation (Hamano *et al*., 2003). The pressure of the ambient gas Ar is 0.02 bar. Thus the pressure of the vapor we observe is expected to change between the two values. In a thermal equilibrium system at high temperatures, most of $SiO_2$ molecules are dissociated to Si and O atoms. As the system cools under an equilibrium, Si and O atoms recombine to SiO and $O_2$ molecules. When the system cools further, almost all of the gas compounds recombine to liquid $SiO_2$. The temperature at which condensation begins depends on pressure: if the pressure of the system is higher, the incipient condensation temperature is higher, and vice versa.

It should be noted that there is always a possibility that ionic compounds are produced by the vaporization of rocks (Kubicki and Stolper, 1993). In our experiment, this translates into the possibility that ionic compounds such as $[SiO_4]^{4-}$ and $Si^+$ were produced. There is also a possibility that clusters will be produced. However, as there is no quantitative thermodynamic data for these ionic compounds and clusters to date, it was not possible to investigate quantitatively the effect of their production on the chemical equilibrium conditions. We use the JANAF table, which is the most recent thermodynamic data available, for the thermodynamic calculations and the interpretation of our experimental data. The calculation of thermodynamic equilibria, including those of ionic compounds and clusters, will be the focus of future investigations.

We did not observe any blackbody radiation in our experiment (Fig. 2(b)–(d)). Thus, laser-induced vapor plumes are most likely to be entirely gaseous. Nevertheless, the absence of strong blackbody radiation cannot fully remove the possibility that there may be some processes that are not observed by visible-light spectroscopy, such as the formation of nano-size particles. Nano-size particles are too small to emit visible blackbody radiation and in our calculation, these are effectively included as condensed phase: $SiO_2$(c) and Si(c). We investigated the possibility that $SiO_2$ condensed in our vapor plume during the spectroscopic observation by comparing the calculated P-T path of the vapor in the experiment with the saturation curve of $SiO_2$.

We first investigated whether $SiO_2$ had already begun to condense immediately after the laser irradiation on the sample. We calculated the initial temperature of the vapor plume by extrapolating the observed temperature as a function of time after the laser irradiation. For the initial pressure, we use the equation between the initial temperature and pressure of a laser-induced vapor plume in Sugita *et al*. (2003). The estimated values are 8600 K and 120 bar; this pressure is lower than the saturation pressure of $SiO_2$ at 8600 K. It is therefore likely that $SiO_2$ did not begin

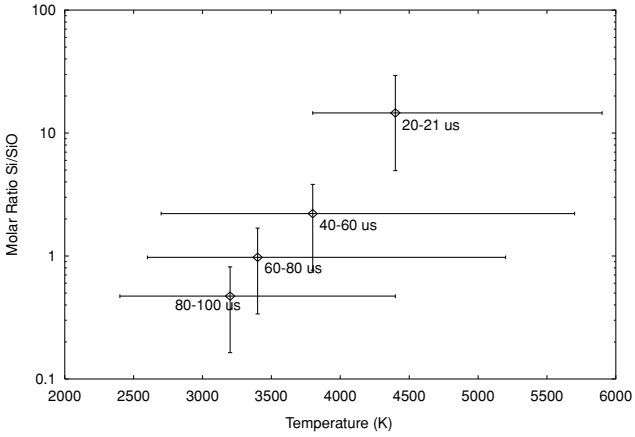


Fig. 12. The number ratio of Si/SiO as a function of temperature. The observation periods for the data points are 20–21 $\mu$s, 40–60 $\mu$s, 60–80 $\mu$s, and 80–100 $\mu$s, respectively from right to left. The vertical error bars indicate the uncertainty of $\tau_{SiO}$ ($0 \sim 0.5$) and that of electronic transition probabilities of the emission line and band. The data points denoted by diamonds on each cross indicate the value when $\tau_{SiO}$ is assumed to be 0.

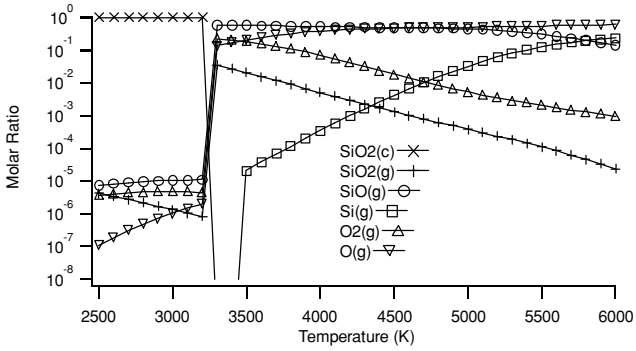


Fig. 13. The molar fraction of each compound under a chemical equilibrium condition. The pressure of the system is fixed at 1 bar.

condensation immediately after the laser irradiation. Alternatively, the plume was most likely gaseous immediately after the laser irradiation and expanded adiabatically without condensation. Condensation starts, however, when the adiabatic curve of the vapor encounters the saturation curve of $SiO_2$. After this, the pressure and temperature of the vapor changes along the saturation curve of $SiO_2$.

We next estimated the temperature at which the condensation began by calculating the adiabatic curve using the initial temperature and pressure estimated above. The specific heat of the vapor changes as chemical reactions proceed. The ratio of specific heats of Si and O atoms are 1.67, and the ratio of specific heat of $SiO_2$ molecule is 1.29. Their recombination reaction is exothermal. Thus, the effective ratio of specific heats is definitely lower than 1.67 and may be slightly lower than 1.29. For the calculation, we assumed that the specific heat of the vapor is constant during the adiabatic expansion. We used different values—from 1.1 to 1.67—for the ratio of specific heat for the calculation. The resulting temperature at which the adiabatic curve encounters the $SiO_2$ saturation curve is between 2000 K and 4000 K. During the spectroscopic observation period

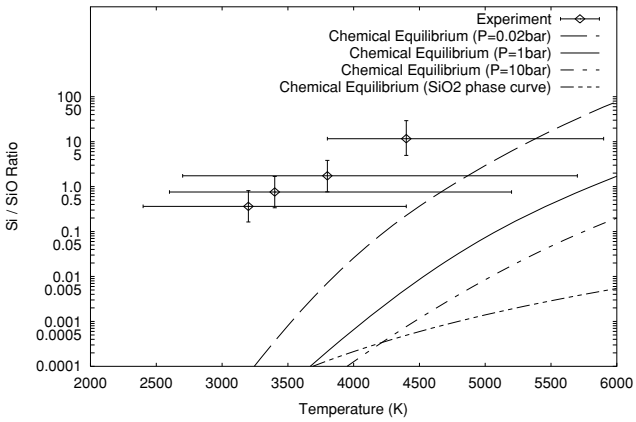


Fig. 14. The number ratio of Si/SiO as a function of temperature. The data points with error bars represent the observed Si/SiO number ratio. The observation periods for the data points are 20–21 $\mu$s, 40–60 $\mu$s, 60–80 $\mu$s, and 80–100 $\mu$s, respectively from right to left. The four lines represent Si/SiO in chemical equilibrium conditions. Constant pressures [0.02 bar (dash line), 1 bar (dot line), and 10 bar (dash-dot line)] and the saturation pressure of $SiO_2$ (dash-dot-dot line) are assumed for calculations. If the vapor observed is in a chemical equilibrium, Si/SiO of the vapor is within the region below the dash line (chemical equilibrium at pressure $= 0.02$ bar). However, the data in the figure show that the Si/SiO ratio is out of any possible equilibrium condition but that it changes from 10 to 0.1 as a function of time. This suggests that Si and O recombine under a non-equilibrium.

(20–100 $\mu$s), the temperature of the vapor decreased from 4400 K to 3200 K. The estimation of the temperature for the beginning of the condensation indicates that there is a possibility that the $SiO_2$ condensation started during the observation period. We therefore took the effect of $SiO_2$ condensation into account when we investigated whether the Si-O recombination process proceeds under a non-equilibrium condition.

### 4.2 The recombination of Si and O under a non-equilibrium condition

In order to understand how Si and O recombine within a high-temperature plume, we compared the observed number ratio of Si to SiO with theoretical estimates based on chemical equilibrium.

There are two possibilities for the expansion of the vapor plume in our spectroscopic observation. One possibility is that the vapor plume expanded adiabatically without condensation. The other possibility is that $SiO_2$ condensation proceeded and that the vapor plume evolved along the saturation curve of $SiO_2$. Taking both these possibilities into account, we investigated whether the Si-O recombination process was consistent with the chemical equilibrium condition.

First, we investigated Si-O recombination process assuming the former possibility. The pressure of vapor expanding adiabatically is higher than the pressure of the ambient Ar atmosphere. Figure 14 shows the number ratio of Si/SiO as a function of temperature. The three lines (dash, dot, and dash-dot) represent the Si/SiO ratio under the chemical equilibrium calculated in Section 4.1. The pressures assumed in the calculations are 0.02 bar, 1 bar, and 10 bar. If the vapor observed is in a chemical equilibrium, the Si/SiO ratio of the vapor is in the region below the dashed line

(chemical equilibrium at pressure of 0.02 bar). However, Fig. 14 shows that all the data points are consistently outside this region throughout the observed time period. Although the upper temperature estimates (i.e., the right end of the error bars) for the first three observation times are below the 0.02 bar line, the vapor plume is likely to be present at higher than ambient pressure (i.e., 0.02 bar) during the early stage of its expansion. Thus, it is very likely that the observed Si/SiO ratio is not in a chemical equilibrium and that the ratio still changes as a function of time.

Here, it is noted that there is a possibility that the formation rates of the $SiO_2$ gas and solid are very slow, leading a non-equilibrium chemical composition. Nevertheless, such a factor actually does not change our conclusion. The number ratio of Si to SiO in the chemical equilibrium calculation not including $SiO_2$ is almost equal to that in the calculation including $SiO_2$. The reason for this is that $SiO_2$ is a very minor component in the gas phase at temperatures and pressures in this study.

We next investigated the Si-O recombination process assuming the latter possibility. If the Si-O recombination proceeded under the equilibrium condition of the experiment, the Si/SiO ratio in the experiment and that in the chemical equilibrium calculation on the $SiO_2$ saturation curve would coincide. The calculated Si/SiO ratio on the $SiO_2$ saturation curve is shown in Fig. 14 as a dash-dot-dot line, and the Si/SiO ratio in the experiment is significantly higher than this line. Models assuming the chemical equilibrium condition cannot explain the Si-O recombination process observed regardless of whether the $SiO_2$ condensation proceeded simultaneously or not. Thus, it is very likely that the Si-O recombination reaction proceeds under a non-equilibrium condition.

The transition from equilibrium to non-equilibrium occurs when the rate of reaction becomes lower than the cooling rate of the vapor. The cooling rate of the vapor in our experiment is temperature-dependent (see Section 3.5). The timescale of cooling is proportional to the temperature to the $-5.7$th power during the observation period between 20 $\mu$s and 100 $\mu$s. The temperature decreases from 4400 K to 3200 K and the cooling timescale increases by a factor of about 6.

The rate of the Si-O reaction is controlled by both the densities of the reactants and the rate constant. The timescale $\theta_{\mathrm{SiO}}$ of the Si-O recombination process is described as

$$\theta_{\mathrm{sio}} = \left( \frac{k_{\mathrm{SiO}}[\mathrm{Si}][\mathrm{O}][M]}{[\mathrm{SiO}]} \right)^{-1} \tag{4}$$

where $k_{\mathrm{SiO}}$ is the rate constant, and $M$ is a third-body molecule/atom. The angular parenthesis in Eq. (4) denotes the densities of the species. If the heat of reaction is emitted as a photon, $[M]$ is not included in Eq. (4).

Since the number ratio [Si]/[SiO] changes from 15 to 0.5, the timescale of the reaction $\theta_{\mathrm{SiO}}$ increases at least 30-fold during the observation period between 20 $\mu$s and 100 $\mu$s. During this same period, the number densities of the O atom and a third particle, if any, are also expected to decrease. This decrease makes the timescale $\theta_{\mathrm{SiO}}$ even longer.

At 20 $\mu$s after irradiation, the vapor is under a non-equilibrium condition (Fig. 14) and $\theta_{\mathrm{SiO}}$ is somewhat longer than $\theta_T$. Between 20 $\mu$s and 100 $\mu$s, $\theta_{\mathrm{SiO}}$ increases at least by a factor of 30, whereas $\theta_T$ increases by only sixfold. If the activation energy of the Si-O reaction is high and, consequently, thus the rate constant $k_{\mathrm{SiO}}$ depends on temperature exponentially, the difference in the two timescales increases exponentially: in other words, the rate of the reaction would very rapidly become lower than the cooling rate of the vapor once the reaction departs from the equilibrium in the cooling vapor.

The experimental results, however, show that the recombination process proceeds even under a non-equilibrium condition, with the number ratio of Si to SiO changing from 15 to 0.5. This strongly suggests that the rate constant for the recombination process is not strongly temperature-dependent; i.e., the effective activation energy of the process is very low. This result is qualitatively consistent with the ab initio calculation of Andreazza *et al.* (1995).

In the system in which the temperature and pressure are decreasing simultaneously, the main cause for the quenching of a reaction is generally the decrease in temperature. However, for a reaction whose activation energy is approximately 0 kJ/mol such as the present Si-O recombination process, the rate coefficient depends only slightly on the temperature. Thus, a sudden decrease in the reaction rate at a certain temperature does not occur. This reaction does not involve quenching at a certain temperature. For such a reaction, decreases in the densities of reactants mainly cause the decrease in the reaction rate. Thus, we do not consider that the Si-O recombination reaction can be explained by a simple 'freeze-out' model in which a chemical reaction suddenly stops at a certain temperature.

## 5. Concluding Remarks

We observed emission spectra of laser-induced quartz vapor to investigate how the rate constant of the Si-O recombination process depends on temperature. We observed blackbody radiation for the plume during the first few microseconds and then atomic lines of Si and molecular bands of SiO in the subsequent 100 $\mu$s. The ratio of intensities of Si to SiO emission changed with time, indicating the recombination of Si and O.

In order to determine the number ratio of Si to SiO, we measured the temperature and the degrees of self-absorption of Si and SiO as functions of time. We used a spectral inversion method to analyze the SiO band emission quantitatively. The result of this analysis shows that Si and O recombined as the vapor cooled from 5000 K to 3000 K.

The thermodynamic calculation of $SiO_2$ vapor was conducted to compare the theoretical value with the empirical results. The comparison strongly suggests that Si and O recombined even under a non-equilibrium condition. Taking the cooling rate of the vapor into consideration, we conclude that the rate constant of the Si-O recombination reaction does not depend on temperature exponentially; its activation energy is approximately 0 kJ/mol in the region between 3000 K and 5000 K.

Such a reaction with a very small activation energy cannot be approximated by a 'freeze-out' model. This simple theoretical model is often used for an impact-induced vapor

plume. However, a quenching process may not work in the Si-O reaction. The oxygen dissociated from $SiO_2$ controls the redox state of the compounds. Therefore, the chemical reaction between Si and O under a non-equilibrium condition needs to be considered when we investigate the chemical evolution of an impact-induced vapor plume on planets and moons.

**Acknowledgments.** The authors wish to thank N. Iwagami and M. Nakamura for their fruitful discussions on the SiO spectrum, T. Kozasa and the late G. Igarashi and for information about kinetic parameters, and S. Ohno for experimental support. The authors also appreciate valuable comments by M. V. Gerasimov, S. Sasaki, and an anonymous reviewer. This research is partially supported by Grant in Aid from Japan Society for the Promotion of Science and Sumitomo Foundation.

## Appendix A. Calculation of synthetic spectrograms of SiO band emission

In Section 3.3, the inversion analysis of SiO band emission is conducted to estimate the temperature and column density of SiO. Sugita and Schultz (2003) describe the procedures to calculate synthetic spectrogram of the $C_2$ band emission. $C_2$ band emission and SiO band emissions are of different types of the electronic transition system. The system of $C_2$ band emission analyzed by Sugita and Schultz (2003) is that of the $C_2$ Swan band system. It is a triplet parallel transition system $A^3\Pi_g \rightarrow X^3\Pi_u$. In contrast, the SiO band emissions we observed are those of the SiO Main system which is a singlet non-parallel transition system $A^1\Pi \rightarrow X^1\Sigma^+$. We describe here the procedures used to calculate synthetic spectrogram of emission bands of the SiO Main system.

Although the SiO band spectrum consists of numerous individual rotational lines (e.g., Herzberg, 1950), it is observed as a continuous spectrum. The wavelength or wave number of each rotational line of a molecular band emission is calculated from the difference in two rotational energy levels. The wave number $\nu$ of a rotational line is given by

$$\nu = T_e' - T_e'' + G'(v') - G''(v'') + F'(J') - F''(J'') \quad \text{(A.1)}$$

where $T_e$ is the energy level of an electronic state at the equilibrium position, $G$ is vibrational energy, $F$ is rotational energy, $\nu$ vibrational quantum number, and $J$ is the total rotational quantum number. A single prime and a double prime denote the upper and the lower states of an electronic transition of molecules, respectively. Note that the energies $T_e$, $G$, and $F$ are in the unit of wave number ($cm^{-1}$). The vibrational energy $G(v)$ is approximated as

$$G(v) = \omega_e\left(v+\frac{1}{2}\right) - \omega_e x_e\left(v+\frac{1}{2}\right)^2 + \omega_e y_e\left(v+\frac{1}{2}\right)^3 \quad \text{(A.2)}$$

where $\omega_e$, $\omega_e x_e$, and $\omega_e y_e$ are vibrational constants. The spin splitting does not exist for the SiO Main system. The effective line wavelength of a singlet transition in the SiO Main system is approximated as

$$F(J) = F(K) = B_v K(K+1) - D_v\left(K+\frac{1}{2}\right)^4 \quad \text{(A.3)}$$

where $K$, $B_v$, and $D_v$ are the rotational quantum number and two rotational constants for the vibrational level of $v$, respectively. The rotational constants $B_v$, and $D_v$ are given by

$$B_v = B_e - \alpha_e\left(v+\frac{1}{2}\right) + \gamma_e\left(v+\frac{1}{2}\right)^2 \quad \text{(A.4)}$$

$$D_v = D_e + \beta_e\left(v+\frac{1}{2}\right) \quad \text{(A.5)}$$

where $B_e$, $D_e$, $\alpha_e$, $\beta_e$, and $\gamma_e$ are rotational constants at the equilibrium position. These constants, which are necessary for the calculation are taken from Lagerqvist *et al.* (1973) and Barrow and Stone (1975).

The spectral radiance $E(\lambda)$ of spontaneous emission from a rotational line is given by

$$E(\lambda) = \frac{4\pi^2 c}{3\,(2J'+1)\,\varepsilon_0\lambda_c^3}\left\{|\mathrm{Re}(\bar{r}_{v'v''})|^2 q_{v'v''}\right\} \times S_{J''\Lambda''}^{J'\Lambda'}\phi(\lambda-\lambda_c)N' \quad (\mathrm{W/m^3/m/sr}) \quad \text{(A.6)}$$

where $\Lambda$ is the resultant orbital angular momentum of the electron along the internuclear axis, $\lambda_c$ is the central wavelength of a rotational line, $\varepsilon_0$ is the dielectric constant of the vacuum, $\bar{r}_{v'v''}$ is the characteristic inter-nuclear separation for the $(v', v'')$ transition ($\gamma$-centroid), $q_{v'v''}$ is the Franck-Condon factor, $S_{J''\Lambda''}^{J'\Lambda'}$ is line strength factor, $|\mathrm{Re}(\bar{r}_{v'v''})|$ is the square of the electronic transition moment, $\phi$ is the line broadening factor, and $N'$ is the number density of SiO in the upper energy level of the transition. Liszt and Smith (1972) calculated the Franck-Condon factor $q_{v'v''}$ of SiO using RKR. Park *et al.* (1993) use the RKR Franck-Condon factor and spectroscopic observation to determine electronic transition moment $|\mathrm{Re}(\bar{r}_{v'v''})|^2$ of the SiO Main system. The line strength factor $S_{J''\Lambda''}^{J'\Lambda'}$ depends on the rotational line branch. If $J' = J'' - 1$, a rotational line belongs to the P branch; if $J' = J''$, it belongs to the Q branch, and if $J' = J'' + 1$, it belongs to the R branch. The strength factor for the P, Q, and R branches, respectively, are given by

$$\text{P branch:}\quad S_{J''\Lambda''}^{J'\Lambda'} = S_{K''\Lambda''}^{K'\Lambda'} = \frac{K'}{2} \quad \text{(A.7)}$$

$$\text{Q branch:}\quad S_{J''\Lambda''}^{J'\Lambda'} = S_{K''\Lambda''}^{K'\Lambda'} = \frac{2K'+1}{2} \quad \text{(A.8)}$$

$$\text{R branch:}\quad S_{J''\Lambda''}^{J'\Lambda'} = S_{K''\Lambda''}^{K'\Lambda'} = \frac{K'+1}{2}. \quad \text{(A.9)}$$

The symbol $K$ denotes the rotational quantum number without spin. For the SiO Main system, $K$ equals to $J$.

The number density $N'$ of SiO in the upper state is given by a Boltzmann distribution if the thermal equilibrium is achieved

$$N' = \frac{N_0 d'\left(2K'+1\right)}{Z(T)} \times \exp\left\{-\frac{hc}{kT}\left(E_e' + G'(v') + F'(K')\right)\right\} \quad (\mathrm{m^{-3}}) \quad \text{(A.10)}$$

where $N_0$ is the total number density of SiO in the all energy levels, $d$ is the electronic multiplicity, and $Z$ is the partition

factor (Arnold *et al.*, 1969). Electronic multiplicity is given by

$$d = \delta\,(2S+1) \tag{A.11}$$

where $\delta$ and $S$ are the lambda doubling factor and quantum number of resultant spin, respectively. For the upper electronic state of the SiO Main system $A^1\Pi$, $\delta$ and $S$ are 2 and 0, respectively.

The partition factor $Z$ of SiO is calculated with

$$Z(T) = \sum_{i=1}^{n}\left[ d_i \exp\left( -\frac{hcT_{e_i}}{kT} \left\{ \sum_{v_J=0}^{v_{J_{\max}}} \frac{kT}{hcB_{v_J}} \times \exp\left( -\frac{hcG(v_J)}{kT} \right) \right\} \right) \right] \tag{A.12}$$

where $v_{J_{\max}}$ is the cut-off vibrational quantum number (Arnold *et al.*, 1969). The cut-off number satisfies either

$$\frac{\exp\left[-\frac{hcG(v_{J_{\max}})}{kT}\right]}{\sum_{v_J=0}^{v_{J_{\max}}} \exp\left[-\frac{hcG(v_J)}{kT}\right]} \le 0.001 \tag{A.13}$$

or

$$G(v_{J_{\max}}+1) \le G(v_{J_{\max}}) \tag{A.14}$$

The rightmost summation of Eq. (A.12) is carried out over 15 electronic states compiled by Huber and Herzberg (1979).

The line broadening in Eq. (A.6) considers both Doppler and collision broadenings. The details are described in Appendix B.

A source spectrum obtained by integration of $E(\lambda)$ in Eq. (A.6) is a spectrum emitted from an optically thin radiation source. In reality, however, the source is altered by the effect of self-absorption because a radiation source has finite optical thickness. The radiance $I$ after self-absorption is given by

$$I(\lambda) = B_T(\lambda)\left[1 - \exp\left(-\frac{E_s(\lambda)l}{B_T(\lambda)}\right)\right] \quad (\mathrm{W/m^2/m/sr}) \tag{A.15}$$

where $B_T$ and $l$ are the blackbody radiation function at temperature $T$ and the thickness of radiation source along the line of sight, respectively (e.g., Arnold *et al.*, 1969). Equation (A.15) assumes that the radiation source is homogeneous and in thermal equilibrium. Incident radiation from outside of the radiation source is also assumed to be negligible. Since radiation sources produced by laser-irradiation are not expected to be homogeneous (Kadono *et al.*, 2002), Eq. (A.15) does not apply in a strict sense. Nevertheless, it should provide a first-order estimate of the spectral characteristics of a radiation source.

The radiance $I$ in Eq. (A.15) is often called a "true spectrum". The effect of finite spectral resolution of the spectrometer needs to be introduced in order to convert a "true spectrum" into a "synthetic spectrum" that can be compared directly with an observed spectrum. A synthetic spectrum is given by a convolution of a true spectrum and the instrumental function of a spectrograph (e.g., Seshadri and Jones, 1963). Since the spectral resolution our spectrometer (FWHM $\sim$ 0.90 nm) is much larger than the width of a typical atomic line, the line profile of an atomic emission line from a Mercury-argon lamp obtained by the spectrometer provides the instrumental function.

## Appendix B. Line broadening of a rotational line of the SiO Main system

In order to calculate a source spectrum of SiO, the line broadening of each rotational line has to be determined. The line broadening includes both Doppler and Lorentz broadenings. The FWHM of Doppler broadening $\sigma_D$ is given by

$$\sigma_D = \frac{2\lambda_c}{c}\sqrt{\frac{2RT\ln 2}{\mu}} \tag{B.1}$$

where $c$, $R$, and $\mu$ are the speed of light, gas constant, and molecular weight of SiO, respectively (e.g., Mitchell and Zemansky, 1961). The FWHM of Lorentz Broadening $\sigma_L$ is derived as

$$\sigma_L = \mathrm{abs}\left[-\frac{1}{\nu_c}\nu\lambda_c\right] = \mathrm{abs}\left[-\frac{\lambda_c}{c}\frac{2\gamma}{2\pi}\lambda_c\right] = \frac{\lambda_c^2}{\pi c}\gamma \tag{B.2}$$

where $\nu$ is the frequency of emission light and $\gamma$ is the collision rate of atoms or molecules. The conversion of $\Delta\nu$ to $\frac{2\gamma}{2\pi}$ is given by the principle of uncertainty. The convolution of Doppler and Lorentz broadenings is given by Voigt function. We use the approximate formula for Voigt function derived by Whiting (1968).

$$\phi(\lambda-\lambda_c) = \phi_{CL}\left\{ \begin{array}{l} \left(1-\frac{\sigma_L}{\sigma_D}\right)\exp\left[-2.772\left(\frac{\lambda-\lambda_C}{\sigma_v}\right)^2\right] \\ +\frac{\frac{\sigma_L}{\sigma_D}}{1+4\left(\frac{\lambda-\lambda_C}{\sigma_v}\right)^2} \\ +0.016\left(1-\frac{\sigma_L}{\sigma_D}\right)\left(\frac{\sigma_L}{\sigma_D}\right) \\ \cdot\left\{\exp\left[-0.4\left(\frac{\lambda-\lambda_C}{\sigma_v}\right)^{2.25}\right] - \frac{10}{10+\left(\frac{\lambda-\lambda_C}{\sigma_v}\right)^{2.25}}\right\} \end{array}\right\} \tag{B.3}$$

where

$$\phi_{CL} = \frac{1}{\sigma_v}\frac{1}{\left[1.065+0.477\left(\frac{\sigma_L}{\sigma_v}\right)+0.058\left(\frac{\sigma_L}{\sigma_v}\right)^2\right]} \tag{B.4}$$

A line width $\sigma_v$ is the Voigt line width and defined as

$$\sigma_v = \frac{\sigma_L}{2} + \sqrt{\left(\frac{\sigma_L}{2}\right)^2 + \sigma_D^2}. \tag{B.5}$$

The collision rate and thus Lorentz broadening due to collision are not straightforward to estimate. Here, we first estimate the collision rate of Si and then that of SiO. The upper limit of the collision rate of Si is obtained from the line width of the observed spectrum, which is the convolution of the true spectrum and the instrumental function. The instrumental width of our spectrometer was 0.90 nm at wavelengths between 250 nm and 600 nm in this study (see Appendix A). However, the measured line width of the observed Si line spectrum at 390.6 nm is 0.90 nm in all the spectrograms, which is indistinguishable from the instrumental width. The pixel resolution of our spectrometer

Table 1. Effective collision cross sections in the vapor plume.

| | Set of particles | collision diameter (Å) | effective collision cross section ($10^{-19}$m$^2$) | reference |
|---|---|---|---|---|
| Dipole-induced dipole interaction | Si-SiO | 10.8 | 9.2 | Park and Arnold (1978) |
| | SiO-O | 10.8 | 9.2 | Park and Arnold (1978) |
| | SiO-$O_2$ | 10.8 | 9.2 | Park and Arnold (1978) |
| | SiO-$SiO_2$ | 10.8 | 9.2 | Park and Arnold (1978) |
| Dipole-dipole interaction | SiO-SiO | 3.7 | 11 | Park and Arnold (1978) |
| Non-dipole-non-dipole interaction | Si-Si | 11.4 | 10.2 | Eq. (B.10) |
| | Si-O | N/A | N/A | |
| | Si-$O_2$ | 10.3 | 8.3 | Eq. (B.10) |
| | O-O | N/A | N/A | |
| | O-$O_2$ | N/A | N/A | |
| | $O_2$-$O_2$ | 9.3 | 6.8 | Eq. (B.10) |
| | $SiO_2$-$SiO_2$ | 8.2 | 5.3 | Eq. (B.10) |
| | Si-$SiO_2$ | 9.8 | 7.5 | Eq. (B.10) |

is within 0.27 nm. Thus the Voigt line width used as that of true spectrum of Si at 390.6 nm is estimated to be smaller than 0.27 nm:

$$\sigma_v < 0.27 \text{ nm}. \tag{B.6}$$

Using Eqs. (B.1), (B.2), (B.5), and (B.6), the collision rate of Si is given as

$$\begin{aligned}\gamma &< \frac{\pi c}{\lambda_c^2}\frac{(0.27\text{ nm})^2 - \left(\frac{2\lambda_c}{c}\sqrt{\frac{2RT\ln 2}{\mu}}\right)^2}{(0.27\text{ nm})} \\ &= 3.5\times 10^{12}\times\left(1.0 - 1.2\times 10^{-8}T\right)\text{ (Hz)}.\end{aligned} \tag{B.7}$$

Thus the upper limit of the collision rate $\gamma_{\max}$ of Si is described as

$$\gamma_{\max\_\mathrm{Si}} = 3.5\times 10^{12}\times\left(1.0 - 1.2\times 10^{-8}T\right)\text{ (Hz)}. \tag{B.8}$$

We consider the cross sections of Si atoms and other atoms and molecules in the vapor plume to estimate the lower limit of the collision rate. The collision rate $\gamma$ in Eq. (B.2) is described as

$$\gamma = v\sum_i N_i Q_i \tag{B.9}$$

where $v$ is the average velocity of Si atoms, $N_i$ is the number density of each chemical composition $i$ in the vapor plume, and $Q_i$ is the effective collisional cross section of Si atoms and other atoms and molecules.

The cross sections of many atoms and molecules have been studied both by theory and experiment. The cross section of atoms (or molecules) depends slightly on the temperature (Park and Arnold, 1978). The collision diameter $D_{\text{collison}}$ of the non-dipole-non-dipole interaction is calculated by the summation of Van der Waals radii of collision partners, $r_{VDW\_1}$ and $r_{VDW\_2}$ (Park and Arnold, 1978):

$$D_{\text{collison}} = 2\left(r_{VDW\_1} + r_{VDW\_2}\right). \tag{B.10}$$

Van der Waals radius of $SiO_2$ is derived from Ahrens and O'keefe (1972): those of Si and $O_2$ are given by Kagaku Binran (1984). The cross sections of the collision expected in the vapor we observed are listed in Table 1. The cross section of Si and $O_2$ is smaller than those of Si and other atoms or molecules. Thus the summation of cross sections in Eq. (B.9) is the smallest when the vapor consists of only Si and $O_2$.

At a lower pressure, the collision rate between atoms and molecules is lower. The lower limit of the pressure is considered to be that of the ambient Ar atmosphere used in our experiment (i.e., 0.02 bar). We use this value to estimate the lower limit of the collision rate of Si.

We use the ideal equation of state for the vapor at the pressure of 0.02 bar and a temperature of over 2500 K. The average velocity of Si, $v$, in Eq. (B.9) is given as

$$\frac{1}{2}\mu v^2 = C_V T \tag{B.11}$$

where $C_V$ is molar heat capacity at a constant volume of Si, $\frac{3}{2}R$. The summation of the number densities of each chemical composition is given as

$$\sum_i N_i = \frac{PN_A}{RT} \tag{B.12}$$

where $N_A$ is the Avogadro number.

Substituting Eqs. (B.11) and (B.12) to (B.9), the lower limit of the collision rate $\gamma_{\min}$ is given as

$$\begin{aligned}\gamma_{\min\_Si} &= Q_{\min}P_{\min}\sqrt{\frac{3}{\mu RT}}N_A \\ &= 3.6\times 10^9\frac{1}{\sqrt{T}}\text{ (Hz)}.\end{aligned} \tag{B.13}$$

Although Si atoms and SiO molecules are in the same vapor, their collision rates are different, with that of Si being

larger than that of SiO. There are two reasons for this. The first is that Si atoms are lighter than SiO molecules and thus move at higher velocities: the atomic weight of Si is 28 and molecular weight of SiO is 44. Using the following equation by Penner (1959), we can estimate that the difference in collision frequency due to the difference in weight is a factor of 1.25:

$$\gamma \propto \frac{P}{\sqrt{T\mu}}. \tag{B.14}$$

Secondly, the cross section between Si and other atoms and molecules is equal to or greater than that of SiO (Table 1). When the vapor is dominated by atoms and nonpolar molecules, the cross section of Si is almost the same as that of SiO. However, if the vapor is dominated by dipole molecules, the cross section of Si is 8.7-fold greater than that of SiO. We do not know the exact chemical composition of the vapor; we only know that Si and SiO exists in the same vapor. Consequently, the collision rate $\gamma_{\mathrm{SiO}}$ of SiO needs to include a free parameter $\beta$,

$$\gamma_{\mathrm{SiO}} = \beta\gamma_{\mathrm{Si}}. \tag{B.15}$$

The value of the ratio $\beta$ ranges from 0.09 to 0.8. Using Eqs. (B.8), (B.13), and (B.15), we obtain the upper limit $\gamma_{\mathrm{max\_SiO}}$ and the lower limit $\gamma_{\mathrm{min\_SiO}}$ of the collision rate of SiO,

$$\gamma_{\mathrm{max\_SiO}} = 0.8 \times \gamma_{\mathrm{max\_Si}} = 3.0 \times 10^{12} \times \left(1.0 - 1.2 \times 10^{-8} T\right) \text{ (Hz)} \tag{B.16}$$

$$\gamma_{\mathrm{min\_SiO}} = 0.09 \times \gamma_{\mathrm{min\_Si}} = 3.2 \times 10^{8} \frac{1}{\sqrt{T}} \text{ (Hz)}. \tag{B.17}$$

Substituting Eqs. (B.16) and (B.17) into (B.2), the upper and lower limits of the Lorentz broadening $\sigma_{L\_\mathrm{max\_SiO}}$ and $\sigma_{L\_\mathrm{min\_SiO}}$ are estimated. For a rotational line of the SiO Main system at 270 nm,

$$\sigma_{L\_\mathrm{max\_SiO}} = 2.7 \times 10^{-10} \times \left(1.0 - 1.2 \times 10^{-8} \times T\right) \text{ (m)} \tag{B.18}$$

$$\sigma_{L\_\mathrm{min\_SiO}} = 2.5 \times 10^{-14} \times \frac{1}{\sqrt{T}} \text{ (m)}. \tag{B.19}$$

Then the maximum and minimum Lorentz/Doppler broadening ratios $\alpha_{\mathrm{max\_SiO}}$ and $\alpha_{\mathrm{min\_SiO}}$ are

$$\alpha_{\mathrm{max\_SiO}} = 9.3 \times 10^{3} \times \left(\frac{1}{\sqrt{T}} - 1.2 \times 10^{-8} \times \sqrt{T}\right) \tag{B.20}$$

$$\alpha_{\mathrm{min\_SiO}} = \frac{0.82}{T}. \tag{B.21}$$

In Section 3.3, the Lorentz/Doppler broadening ratio $\alpha$ is used as a free parameter to explain the methods and results of our analysis. Since the temperature of the vapor ranges from 3000 K to 5200 K, the range of $\alpha$ is about 0.0001 to 150.

The effect of the line broadening is calculated up to 10 Voigt widths away from the center of the line. In the optimum case, the error due to this truncation is $10^{-6}$ for the Voigt width equal to the Lorentz width. In the worst case, the error is 6.3% for the Voigt breadth equal to the Doppler breadth (Whiting, 1968). The Doppler widths of Si and SiO are larger than $10^{-3}$ nm for the wavelength range between 250 mm and 300 nm when the temperature is higher than 2000 K. Consequently, in our study, we used a wavelength increment of $10^{-4}$ nm and reconstructed the precise profile of a spectral line.

## References


Andreazza, C. M., P. D. Singh, and G. C. Sanzovo, The radiative association of C and S, $C^+$ and S, Si and O, and $Si^+$ and O, *Astrophys. J.*, **451**, 889–893, 1995.

Arnold, J. O., E. E. Whiting, and G. C. Lyle, Line by line calculation of spectra from diatomic molecules and atoms assuming a voigt line profile, *J. Quant. Spectrosc. Radiat. Transfer*, **9**, 775–798, 1969.

Ahrens, T. J. and J. D. O'keefe, Shock melting and vaporization of lunar rocks and minerals, *Moon*, **4**, 214–249, 1972.

Barrow, R. F. and T. J. Stone, The identification of a new band system associated with gaseous silicon monoxide, *J. Phys.*, **B8**, L13–L15, 1975.

Basaltic Volcanism Study Project (BVSP), *Basaltic Volcanism on the Terrestrial Planets*, Pergamon, 1286 pp., New York, 1981.

Cannon, C. J., *The Transfer of Spectral Line Radiation*, 541 pp., Cambridge Univ. Press, New York, 1985.

Chase, M. W., Jr., C. A. Davies, J. R. Downey, Jr., D. J. Frurip, R. A. McDonald, and A. N. Syverud, JANAF Thermochemical Tables 3rd edition, *Journal of Physical and Chemical Reference Data, 14 Supplement No. 1*, 1856 pp., 1985.

Divine, N., Five populations of interplanetary meteoroids, *J. Geophys. Res.*, **98E9**, 17029–17048, 1993.

Fegley, B., Jr., R. G. Prinn, H. Hartman, and G. H. Watkins, Chemical effects of large impacts on the earth's primitive atmosphere, *Nature*, **319**, 305–308, 1986.

Griem, H. R., *Plasma Spectroscopy*, 580 pp., McGraw-Hill, New York, 1964.

Kadono, T., S. Sugita, N. K. Mitani, M. Fuyuki, S. Ohno, Y. Sekine, and T. Matsui, Vapor clouds generated by laser ablation and hypervelocity impact, *Geophys. Res. Lett.*, **29**(20), 1979–1982, 2002.

Kubicki, J. D. and E. M. Stolper, Evaporation kinetics of $Mg_2SiO_4$ crystals and melts from molecular dynamics simulations, *Lunar Planet. Sci. Conf. XXIV*, no. 829, 1993.

Hamano, K., S. Sugita, T. Kadono, and T. Matsui, A new method to measure the pressure of impact-induced vapor clouds, *Lunar Planet. Sci. Conf. XXXIV*, no. 1647, 2003.

Herzberg, G., *Molecular Spectra and Molecular Structure, I, Diatomic Molecules*, 2nd ed., 678 pp., D. Van Nostrand, New York, 1950.

Huber, K. P. and G. Herzberg, *Molecular Spectra and Molecular Structure VI. Constants of Diatomic Molecules*, 716 pp., Van Nostrand-Reinhold, New York, 1979.

Lagerqvist, A., I. Renhorn, and N. Elander, The spectrum of SiO in the vacuum ultraviolet Region, *J. Molec. Spectrosc.*, **46**, 285–315, 1973.

Langhoff, S. R. and J. O. Arnold, Theoretical study of the $X^{1+}$, $A^1$, $C^{1-}$, and $E^{1+}$ states of the SiO molecule, *J. Chem. Phys.*, **70**(02), 853–863, 1979.

Liszt, H. S. and W. H. Smith, RKR Franck-Condon factors for blue and ultraviolet transitions of some molecules of astrophysical interest and some comments on the interstellar abundance of CH, $CH^+$ and $SiH^+$, *J. Quant. Spectrosc. Radiat. Transfer*, **12**, 947–958, 1972.

Mitchell, A. C. G. and M. W. Zemansky, *Resonance Radiation and Exited Atoms*, 338 pp., Cambridge University Press, London, 1961.

Mukhin, L. M., M. V. Gerasimov, and E. N. Safonova, Origin of precursors of organic molecules during evaporation of meteorites and mafic terrestrial rocks, *Nature*, **340**, 46–48, 1989.

Park, C., High temperature reformation of aluminum and chlorine compounds behind the mach disk of a solid-fuel rocket exhaust, *Atmos. Environ.*, **10**, 693–702, 1976.

Park, C. and J. O. Arnold, A shock-tube determination of the SiO($A^1\Pi$-$X^1\Sigma^+$) transition moment, *J. Quant. Spectrosc. Radiat. Transfer*, **19**, 1–10, 1978.

Park, C. S., D. R. Crosley, D. J. Eckstrom, and K. R. Heere, Measurement of the $A^1\Pi$-$X^1\Sigma^+$ electronic transition moment of SiO using a shock-tube, *J. Quant. Spectrosc. Radiat. Transfer*, **49**(4), 349–360, 1993.

Penner, S. S., *Quantitative Molecular Spectroscopy and Gas Emissivities*,

578 pp., Addison-Wesley, London, 1959.

Sasaki, S., K. Nakamura, Y. Hamabe, E. Kurahashi, and T. Hiroi, Production of iron nanoparticles by laser irradiation in a simulation of lunar-like space weathering, *Nature*, **410**, 555–557, 2001.

Seshadri, K. S. and R. S. Jones, The shapes and intensities of infrared absorption bands-A review, *Spectrochim Acta*, **19**, 1013–1085, 1963.

Sugita, S. and P. H. Schultz, Interaction between impact-induced vapor clouds and an atmosphere 1: Spectroscopic observation, *J. Geophys. Res.*, **101E6**, 2003.

Sugita, S., P. H. Schultz, and M. A. Adams, Spectroscopic measurements of vapor clouds due to oblique impacts, *J. Geophys. Res.*, **103E8**, 19,427–19,441, 1998.

Sugita, S., T. Kadono, S. Ohno, K. Hamano, and T. Matsui, Does laser ablation vapor simulate impact vapor?, *Lunar Planet. Sci. Conf. XXXIV*, no. 1573, 2003.

The Chemical Society of Japan, *Kagaku Binran Kisohen II Kaitei 3 ban*, Maruzen, 1984.

Whiting, E. E., An empirical approximation to Voight profile, *J. Quant. Spectrosc. Radiat. Transfer*, **8**, 1379–1384, 1968.

Wiese, W. L. and G. A. Martin, *Wavelength and Transition Probabilities for Atoms and Atomic Ions, Part II. Transition Probabilities*, 359–406, National Bureau of Standards, Washington D.C., 1980.

M. Fuyuki (e-mail: fuyuki@clusterlab.jp), S. Sugita, T. Kadono, S. Hasegawa, and T. Matsui